International Journal of Intelligent Robotics and Applications
https://doi.org/10.1007/s41315-024-00352-z

REGULAR PAPER

Implementation of extended kalman filter for localization of ambulance robot

Chan-Yun Yang[1] · Hooman Samani[2] · Zirong Tang[3] · Chunxu Li[3]

Received: 13 April 2024 / Accepted: 7 June 2024

Abstract
This paper focuses on the implementation of the Extended Kalman Filter for indoor localization of a semi-autonomous Ambulance Robot system named Ambubot. The system is designed to reduce the response time for lay rescuers to locate an Automated External Defibrillator (AED) during sudden cardiac arrest events. To achieve this objective, the robot is equipped with an AED, and the Extended Kalman Filter is utilized for optimal indoor localization. The filter is implemented using data from the robot's Inertial Measurement Unit, which comprises 9 Degrees of Freedom. The paper provides an explicit description of the performance of the Extended Kalman Filter in estimating the position of Ambubot, and demonstrates that the proposed approach is effective in accurately determining and estimating the robot's position in unknown indoor environments. The results suggest that the proposed method is a promising solution for improving survival rates in cardiac arrest cases, and may have potential applications in other fields where accurate indoor localization is required.

Keywords Extended kalman filter · Localization · Intelligent system · Autonomous robot

1 Introduction

Emergency situations can occur unexpectedly at any time, and they can cause signifi-cant harm to people's lives. While the number of reported deaths due to natural calamities appears to be decreasing according to data from The International Disaster Database (EM-DAT) (Moraes and Luiz 2022), the number of people affected by natural disasters is increasing dramatically. Therefore, reducing the mortality rate is generally regarded as the most effective approach. In such emergencies, timely medical intervention is critical to saving lives and minimizing harm.

When there is a sick or injured person requiring immediate assistance, we typically dial an emergency number to request help. Once the emergency is confirmed, an ambulance is dispatched to the scene, with an average response time of ten minutes, as depicted in Fig. 1 for various regions (Liu et al. 2022). In reality, the ambulance's arrival time often exceeds the ten-minute standard in many cases due to various obstructions during the dispatch process, which may cause a delay in receiving timely services for the patient. Factors contributing to this issue include traffic congestion, difficulty in locating the address, long distances, and so on. Any of these delays can result in a longer response time.

The prompt transportation of patients to the hospital by ambulance is of utmost importance, particularly in life-threatening emergency situations. However, in some cases, patients require emergency treatment at the scene before transportation to the hospital, such as in cases of sudden cardiac arrest. The timely application of treatments such as Automated External Defibrillator (AED) can significantly improve patient outcomes. AEDs are small, portable defibrillators designed for use by minimally trained or untrained non-medical personnel (Karlsson et al. 2020). These devices can generate both single-phase and double-phase waveforms. While single-phase waveforms can produce a

✉ Chunxu Li
chunxu.li@swansea.ac.uk

[1] Department of Electrical Engineering, National Taipei University, Taipei, Taiwan

[2] Creative Computing Institute, University of the Arts London, London SE5 8UF, UK

[3] Department of Mechanical Engineering, Faculty of Science and Engineering, Swansea University, Swansea SA1 8EN, UK

Published online: 25 June 2024

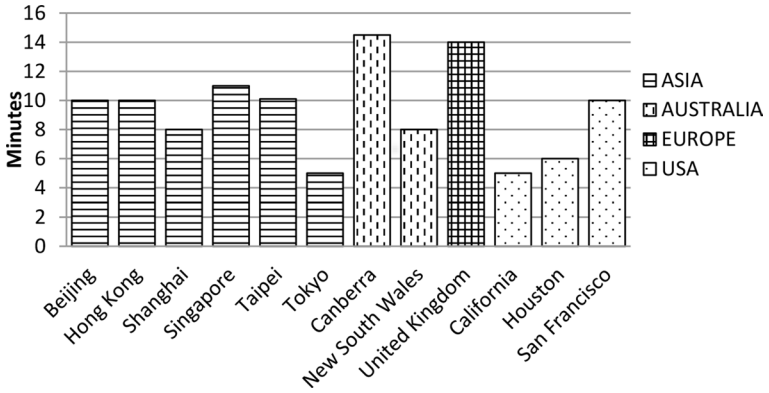

Fig. 1 Response Times of Ambulance Services in Various Territories

high-energy output that can cause damage to the heart and skin, double-phase waveforms generate a low energy output that shocks the heart twice simultaneously, thereby reducing the complications associated with defibrillation.

In accordance with AED guidelines, it is recommended that the person rendering assistance immediately call for an ambulance prior to administering the AED. In situations where two individuals are present, one should call for an ambulance while the other manages the AED. Although laypeople are able to use this device to provide initial aid to a victim experiencing cardiac arrest, it would be preferable for a person who has completed first aid training to operate it. Despite the fact that AEDs are widely available in public places, locating them during an emergency is challenging in practice (Rothmier and Drezner 2009). This difficulty is often exacerbated by initial panic that occurs when individuals are faced with such circumstances. To address these challenges and ensure patients remain alive until the arrival of the ambulance, we have developed the Ambulance Robot (Ambubot (Samani and Zhu 2016) application, which carries an AED and, according to our long-term plans, is able to perform CPR on an individual experiencing cardiac arrest.

Ambubot, equipped with tele-operated capabilities, is capable of navigating challenging indoor and outdoor terrains to locate the victim. This robot can effectively communicate with human rescuers to gather important information, such as the location of the victim on a map, and the best way for human rescuers to reach the victim (Arif and Samani 2014). Additionally, Ambubot can address the constraint of human limitations in locating the nearest AED to the victim, thereby increasing the victim's chances of survival. In navigating the environment, the robot must determine its locomotion before moving to different positions, given that it lacks prior knowledge of its initial position and must therefore self-localize from scratch. Ambubot must integrate advanced navigation and positioning systems to overcome the challenges of self-localization and effectively perform its rescue operations. Therefore, achieving precise positioning of the robot is a key issue to be addressed in this article.

Inertial Navigation Systems (INS) and Global Positioning Systems (GPS) are utilized to provide precise and reliable navigation and positioning in applications such as aerospace, maritime, military, and autonomous vehicles (Zhang et al. 2021; Cheng et al. 2024). It is known that GPS-like signals are susceptible to interference or loss due to the limitations of electromagnetic waves (Hu et al. 2023). Additionally, small errors in angular velocity and acceleration measurements consolidate into larger errors in velocity and position. Due to these limitations, some scholars have proposed efficient sensor fusion algorithms and methods based on the Kalman filter (Lyu et al. 2024). To improve the accuracy of autonomous driving navigation information, a navigation technology based on an adaptive Kalman filter with an attenuation factor has been proposed to suppress noise. According to test results, the accuracy of the proposed algorithm is 20% higher than that of a traditional adaptive Kalman filter (Liu et al. 2018).

Since the standard Kalman filter is only applicable to linear systems, and the actual systems we encounter often have certain nonlinear characteristics. Bucy and Sunahara performed a nonlinear extension of the Kalman filter algorithm and proposed the famous Extended Kalman Filter (EKF). For systems with lower dimensions and weak nonlinearity, the Extended Kalman Filter is widely used because of its simple algorithm structure, small computational load, and minimal linearization error (Xu et al. 2023).

In this study, we have employed the Extended Kalman Filter (EKF) technique for the Ambubot to determine its locomotion. The Inertial Measurement Unit (IMU) with 9 degrees of freedom, including a 3-axis accelerometer, 3-axis gyroscope, and 3-axis compass, is utilized to gather data related to the Ambubot. The implementation of the Extended Kalman Filter is described explicitly in Matlab through offline data. Subsequent sections of the paper will provide a detailed explanation of this research. The remainder of the paper is organized as follows: Sect. 2 presents the robot model and sensor device equipment. Section 3 outlines the adaptive algorithm of EKF. Section 4 describes the

experimental tests carried out on Matlab. Finally, in Sect. 5, concluding remarks are provided.

2 The mobile robot-ambubot

Ambubot (Samani and Zhu 2016), a mobile robot with a simple design, is designed to operate efficiently in indoor and outdoor environments with rapid maneuverability. The robot is equipped with a 9 DOF IMU (Gyro/Accelerometer/Compass) and outdoor GPS for autonomous navigation. Its weather and water-resistant features coupled with a low power consumption rate make it a highly advantageous device. Furthermore, its compact size allows for a large payload capacity and its light gripper can lift objects up to 10 kg. The gripper's functionality extends to handling, object inspection, and an articulated sensor platform. Ambubot's two high-resolution video cameras offer the operator a remote zoom-in and zoom-out functionality to enhance object visibility. Its four powerful motors, one for each wheel, enable it to move faster than its contemporaries. The key components of Ambubot are illustrated in Fig. 2.

As previously mentioned, Ambubot was utilized as a platform for saving the life of an individual experiencing cardiac arrest. Two methods were employed to achieve this, namely a body-attached sensor and a mobile phone application, as depicted in Fig. 3. When either of these techniques was activated, a warning message and GPS information were immediately transmitted to the Ambubot center. Subsequently, the center utilized a GPS and GIS parser to convert the received longitude and latitude coordinates into a street map location. Additionally, the location data was integrated with other pertinent information such as personal contacts and characteristics, blood type, height, weight, and photograph to generate the necessary data required to assist the victim.

After processing the data packet, the Ambubot center generated two commands, namely a dispatch command, which directed Ambubot to move from the station to the location of the incident as a precautionary measure to save the patient's life before the arrival of the ambulance, and another command, which sent an emergency message to family members through the Global System for Mobile Communication (GSM) network. In the case of victims with the body-attached sensor, family members would receive an alert message containing relevant information concerning the fallen individual via their mobile phones. Furthermore, confirmation of the incident would prompt informing the nearest hospital's ambulance. Ambubot has a maximum speed of 10 km/hour and can pass slopes of up to 45 degrees. With its faster maneuverability, the robot is capable of traversing rough terrain and ascending staircases to mitigate the ambulance's delay.

The body-attached sensor, which is a crucial component in the life-saving system, comprises a GPS satellite location module, a gyro sensor, a microprocessor, and a GSM communication module, as depicted in Fig. 4. To ensure that the body-attached sensor does not impede the daily lives of individuals, it is integrated into frequently used objects such as glasses frames, belts, and watches. The sensor is designed with dimensions that are suitable for attaching it to the human body, and it consumes minimal power. Additionally, a tag that contains the patient identification code is concatenated with the body-attached sensor. When a patient is registered, the identification code can be used to retrieve information such as their name, date of birth, age, photographs, relatives' contact information, and personal health history from Ambubot center, which is critical for ensuring the patient's safety. The microprocessor is the primary intelligent hardware module responsible for computation, while the GSM communication module facilitates communication between the sensor and Ambubot center for transmitting

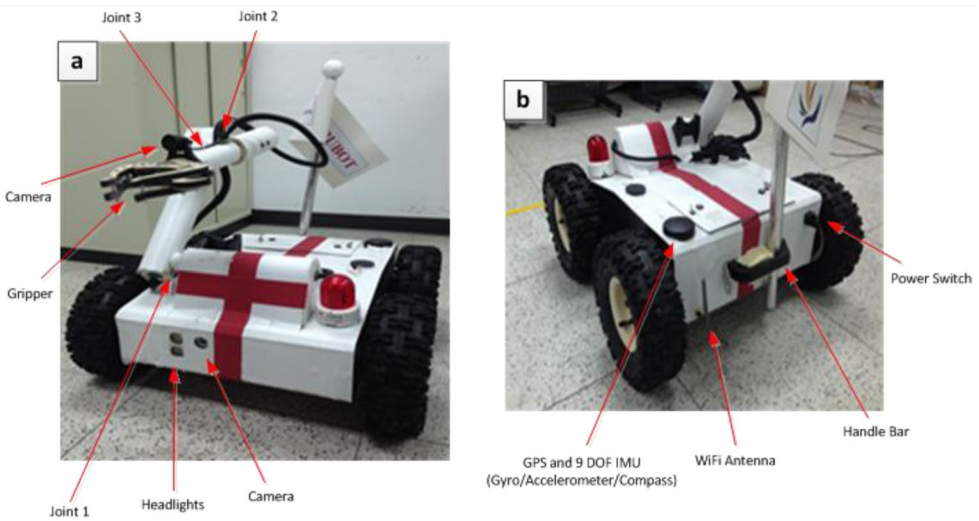

Fig. 2 General structure of Ambulance Robot (Ambubot) (**a**) Front view (**b**) Side view

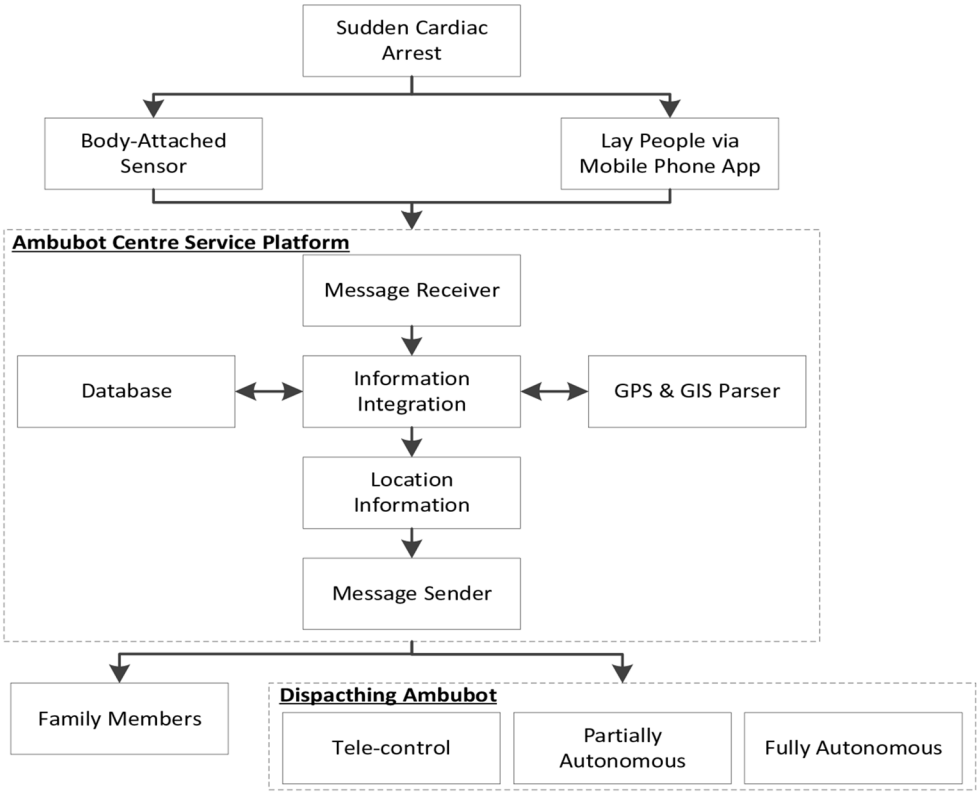

Fig. 3 Overview of the system workflow

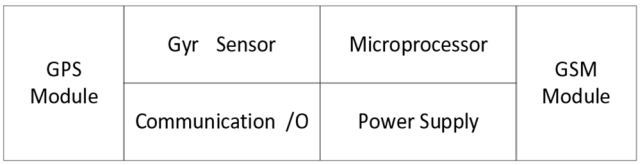

Fig. 4 Block diagram of body-attached sensor

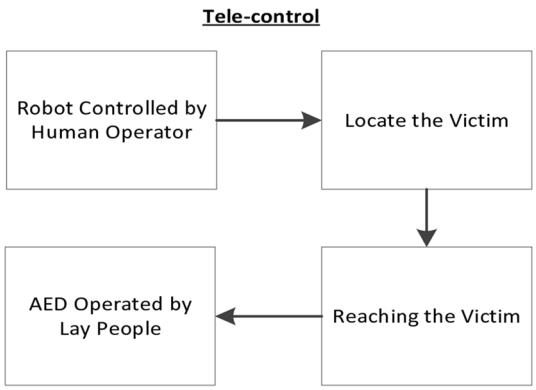

Fig. 5 Workflow of the search assistance for tele-control

emergency rescue messages and receiving commands. To ensure proper functioning of the body-attached sensor, it is vital to have a power supply that can provide the appropriate amount of power. The sensor sends a message to family members to replace the battery when only 10% of the power remains, to ensure the system's normal operation. Ambubot can be dispatched to a destination using various methods, such as tele-control, partially autonomous, or fully autonomous, which are detailed below.

2.1 Tele-control

Tele-control is a system that aids human operators in directing the maneuvering of Ambubot via a visual display and a control pad. The proposed tele-control system's overview is depicted in Fig. 5. Generally, the primary function of a tele-control system is to help human operators perform and complete complex and uncertain tasks in hazardous and less structured environments. In this method, an Ambubot requires a human driver who is responsible for controlling the robot using a remote control device, which is similar to a controller panel, and monitoring the real-time video stream from two surveillance cameras on the Ambubot. In this scenario, when Ambubot approaches the victim, human operators from the control center give detailed instructions to people in the vicinity of the victim to operate the AED device, which is carried by Ambubot.

2.2 Partially autonomous

Partially autonomous mode combines the autonomous functions of the robot with direct maneuvering by human operators. The robot can perform some tasks autonomously, but

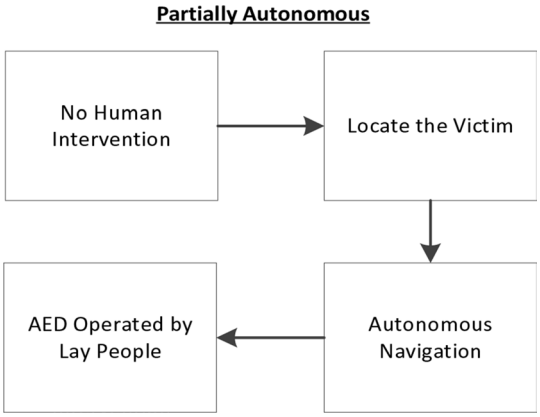

Fig. 6 Workflow of the search assistance for partially autonomous

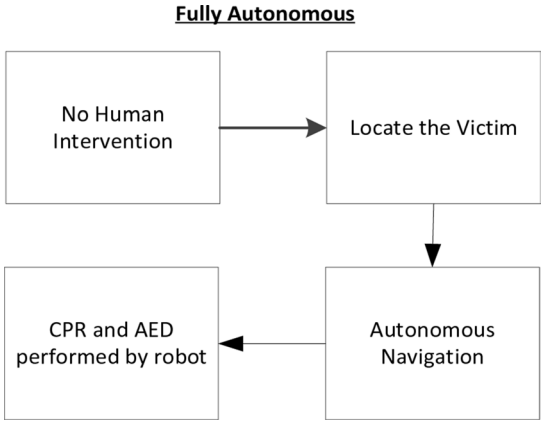

Fig. 7 Workflow of the search assistance for fully autonomous

human intelligence and flexibility are still needed to adjust the task procedures to the real environment and ensure safety. In this mode, when Ambubot center receives GPS information regarding the victim, the server computes the shortest path and transmits it to the robot. Ambubot then navigates autonomously while avoiding obstacles and streams video through two cameras mounted on the robot to display its motion (Arif et al. 2012). This operation method can improve navigation and reduce stress for the operators. However, human intervention is still needed to provide additional information to the robot based on the circumstances. In the case of cardiac arrest, humans near the victim still play an important role in applying the pads of AED on the victim's chest (Fig.6).

2.3 Fully autonomous system

As discussed previously, Ambubot can be dispatched through tele-control or partially autonomous methods. However, the most advanced method involves a fully autonomous navigation system that delivers an AED to the victim's location and operates it without the need for continuous human guidance. This approach differs from the previous sections where lay rescuers applied the pads of the AED themselves on the victim's chest. In future plans, Ambubot could also perform CPR as the first aid to save the victim's life in cardiac arrest. The Ambubot grabber has been designed to be light enough to apply the AED pads to the victim's chest and strong enough to withstand the weight of the AED. Nonetheless, an obstacle may arise when the victim is in an unsuitable posture to apply the AED (see Fig.7).

2.4 System architecture

During the development of Ambubot, we prioritized the partially autonomous method which involves a robot stationed in a central location and a control server equipped with a computer. The Ambubot center service platform consists of three servers: the database server, message controller server, and GIS server, as depicted in Fig. 8. All three servers are located within a firewall to ensure system security. The database server is designed to store and manage data, while the message controller server is linked to the telecom's short message server to improve message processing efficiency, including the acceptance and transmission of a large volume of short messages through network packets. The GIS server is responsible for converting GPS longitude/latitude coordinates into location information such as street addresses and landmarks, enabling family members and Ambubot to acquire geographic spatial information about the fallen patient and dispatch Ambubot more effectively. Additionally, this server is solely responsible for assisting Ambubot in finding the possible shortest path between itself and the victim.

The system's connectivity to the GSM network enables it to address the issue of invalid GPS signals. The system utilizes the GSM-locating service offered by a local GSM network company to track the victim's location. While the location of the victim may not be pinpointed accurately, this approach resolves the challenge of locating the victim in adverse weather conditions.

The block diagram depicted in Fig. 9 illustrates the practical implementation of dispatching Ambubot to the scene. The telepresence technique enables an operator to control Ambubot remotely and guide it to the victim's location. Two applications, namely body attached sensors and a mobile phone application, work in tandem to generate an emergency message along with the current position of the victim. The generated data is automatically evaluated and transmitted to Ambubot center without any delay as soon as a sudden cardiac arrest occurs.

With the widespread use of smart mobile phones, the development of a mobile phone application that connects to the Ambubot center has become a convenient means of

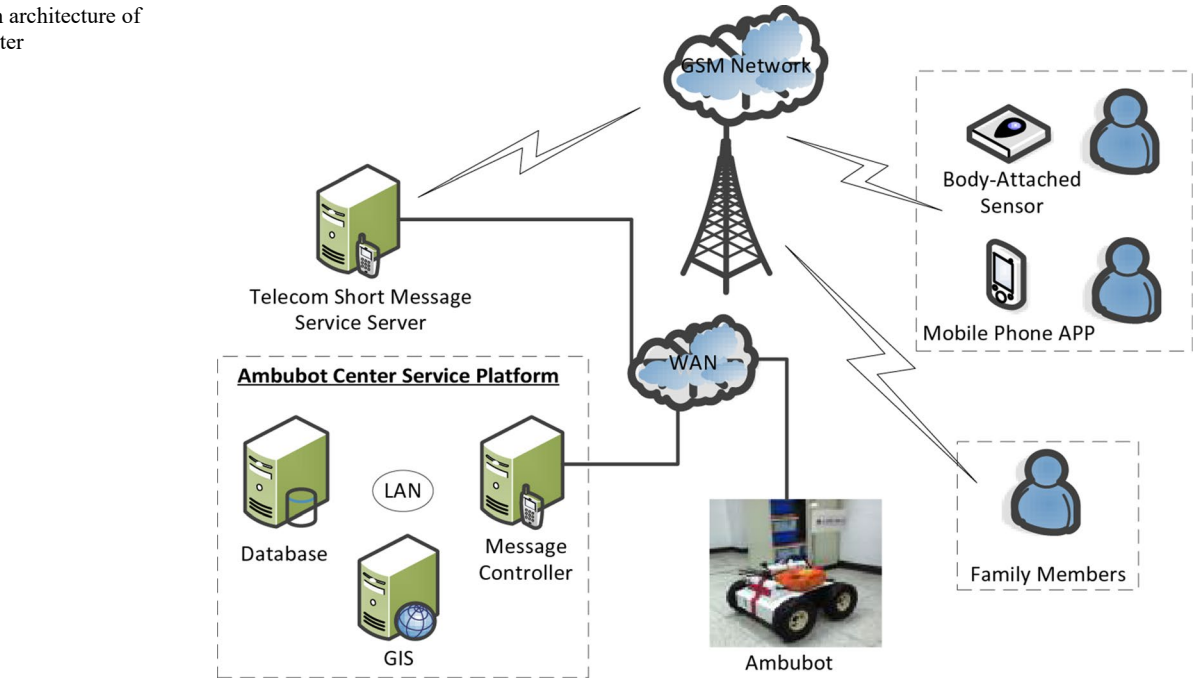

Fig. 8 System architecture of Ambubot center

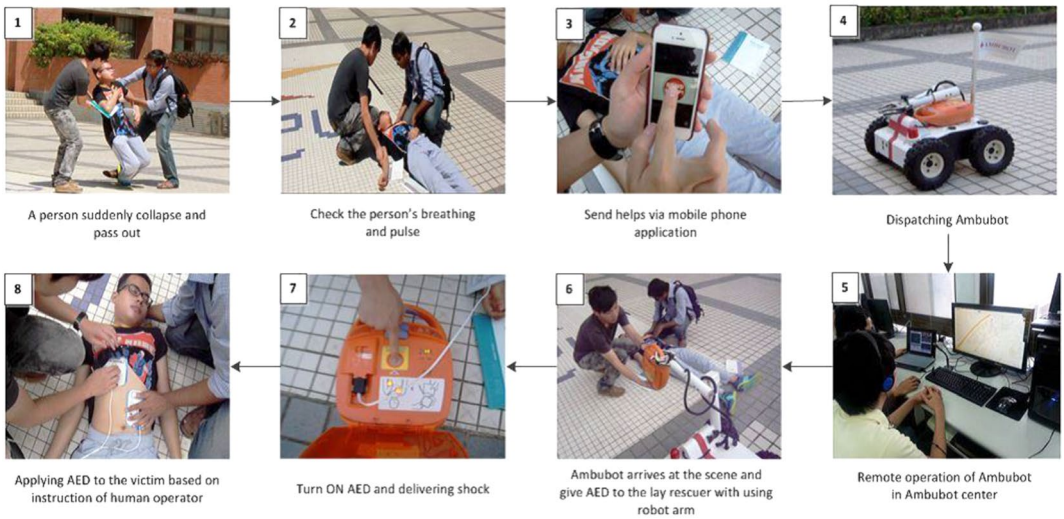

Fig. 9 The entire scenario of dispatching Ambubot to the scene

providing timely medical care to the victim. However, in the case of a lack of a smart phone, calling the center can serve as an alternative method. The Ambubot center stores the history of the victim during the cardiac arrest in the database server, which is extremely useful for family members to gain new insights and understand the victim's healthcare. Once the GIS server obtains the location information of the victim, it tracks down the victim's location and converts it into important landmarks, thereby producing highly precise and accurate information about the victim's current position. Subsequently, the history and location information of the victim are integrated with the message controller server.

The GIS server, upon obtaining accurate location information of the victim, will integrate this data with the message controller server, which in turn will connect to the telecom's short message server to send a message to the victim's family members. The message will include important details about the victim, such as personal contacts, physical characteristics, blood type, height, weight, photograph, and medical history during cardiac arrest. Ambubot will then be dispatched to the scene based on the received information.

Although Ambubot has the capability to perform simple tasks autonomously, it still requires human intervention in the event of communication failure. This can be achieved through a control pad or computer, as illustrated in Fig. 10.

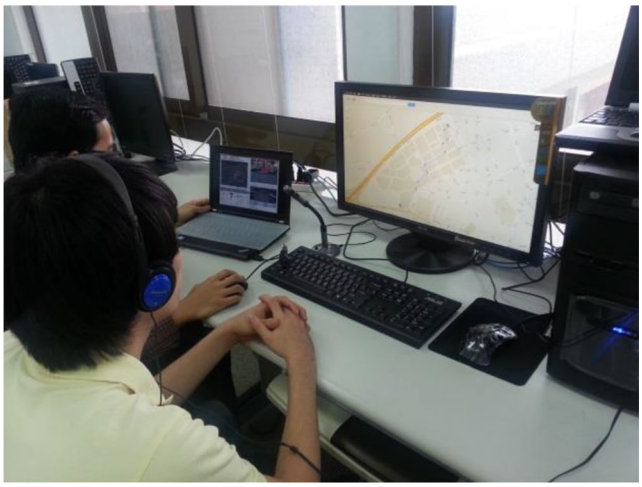

Fig. 10 Remote operation of Ambubot in Ambubot center

Additionally, as depicted in Fig. 11, Ambubot is equipped with high-resolution video and audio capabilities, allowing human operators to obtain detailed information about the surroundings. Upon reaching the victim's location, the human operator instructs lay rescuers on how to apply the AED pads to the victim's chest.

3 Position estimation with an extended kalman filter

The Kalman Filter (KF) is a recursive algorithm that can estimate the state variables of a dynamic system by integrating all available measurements and providing a least squares estimate of a process state (Bai et al. 2023; Xiao et al. 2024). This algorithm is particularly useful in estimating the state variables of a noisy linear dynamical system, even when the modeled system is unknown (Zanetti et al. 2009). In the present study, the Extended Kalman Filter (EKF) has been selected as a pervasive tool for implementation in Ambubot, specifically in the domain of navigation and global positioning.

The loop of Ambubot is composed of three modules: the control or vehicle path module, the observation module which utilizes the IMU sensor, and the estimation module utilizing EKF. The IMU sensor on Ambubot has 9 degrees of freedom, allowing it to output roll, pitch, and yaw estimates. The accelerometer generates pitch estimates, the gyroscope generates roll estimates, and the compass generates yaw estimates. The complete loop of Ambubot is illustrated in Fig. 12.

3.1 Control module

The input of the control module is the angular position provided by the estimation module. By using the two-stage correction and quaternion approaches, the angular position can be efficiently adjusted in the system. The primary objective of the control module is to aid Ambubot in following an intended path by utilizing the knowledge of the angular position and a set of predefined routines, namely GoPoint and FollowPath.

The GoPoint routine enables Ambubot to reach a specific point in space. The control module also features the FollowPath routine that enables Ambubot to follow a path.

Fig. 11 Ambubot controller interface

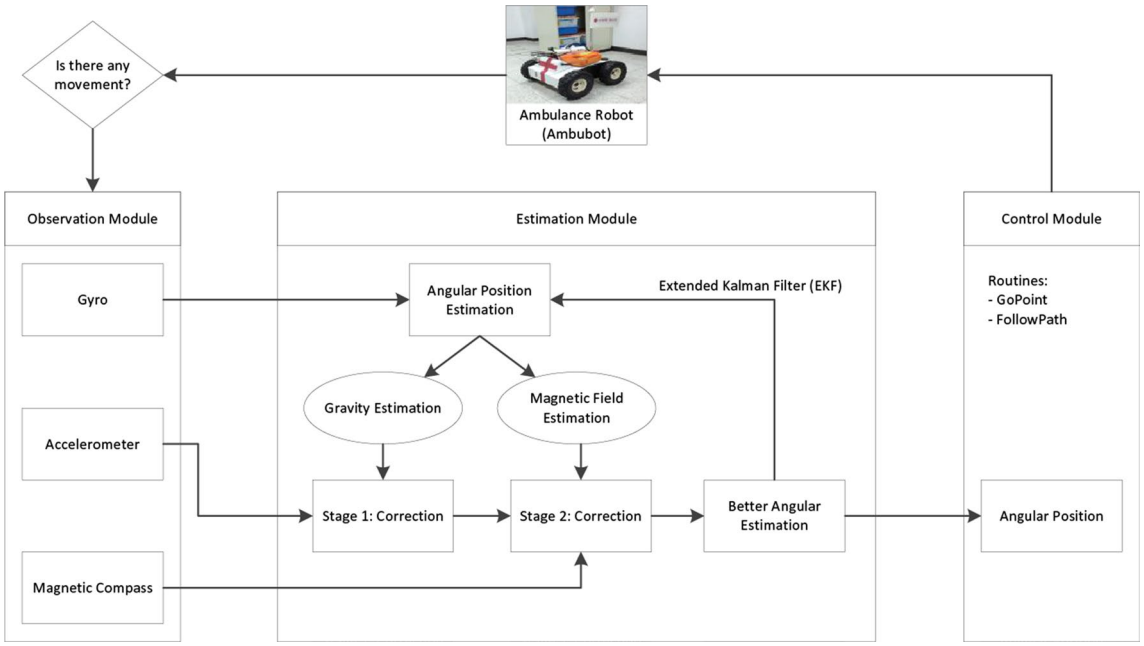

Fig. 12 Sensor fusion algorithm principles for Ambubot

The linear velocity is the output of these routines, and the velocity of each wheel is determined using the following equations:

$$V_{right} = \frac{2\pi R_{right} n_{right}}{NT} \tag{1}$$

$$V_{left} = \frac{2\pi R_{left} n_{left}}{NT} \tag{2}$$

where R_{right} and R_{left} are the radii of the right and left wheels, n_{right} and n_{left} are the pulse frequencies for the right and left wheels, N is the motor resolution (pulse per revolution) and lastly, T is the gear ratio from the driving motor to the wheels (Hardt et al. 1994).

3.2 Observation module

In this particular module, we utilized the IMU sensor of Ambubot, which provides accurate, reliable, and wide-ranging sensor data, to obtain full 9 degrees of freedom. During the initial movement of Ambubot, three distinct input data types, namely the gyroscope, accelerometer, and magnetic compass, were employed. The gyroscope measured the angular rate on each of the three axes in degrees or revolutions per second (Chang et al. 2010) and also served as an input to update the angular position. The accelerometer, on the other hand, measured the acceleration in grams, while the magnetic compass data measured the magnetic field in gauss (Tan and Park 2005; Bird and Arden 2011). Inaccuracies in the angular position estimation were subsequently rectified using data from both the accelerometer and magnetic compass, which functioned as fixed references.

The observation module started with defining a discrete-time state equation $\widehat{x_k^-}$ that describes the evolution of the system state x_k. It is started from the system state at the previous step x_k. with the evolution law described by the matrix A_k and responding to some system inputs u_k. with the evolution law B_k.. Accordingly, this equation can be written as

$$\widehat{x}_k^- = A_k \widehat{x}_{k-1} + B_k u_k \tag{3}$$

Equation (2) is called priori system state estimation. It is denoted by superscript minus and by the hat on the system state x_k. Those signs represented by this equation aim to describe that the real system state is unknown. Therefore, the Kalman Filter is used to provide estimation.

3.3 Estimation module

In order to represent the angular position as system state, we used the quaternion in the state equation. With using quaternion, the system can be better linearized despite the fact that the inclusion of other variables in the system state leads to greater processing power (Kim and Golnaraghi 2004; Yuri et al. 2008). Further, it does not significantly improve accuracy of the angular estimation. On the other hand, it tends to make bigger matrix operations. The angular position is represented using a quaternion q

$$q = [q_0, q_1, q_2, q_3]^T \tag{4}$$

where q_0. represents the real number, and $v = [q_1, q_2, q_3]^T$ represents the vector.

A rotation can be uniquely defined by the axis of rotation, in this case vector *v*, and by the angle of rotation α around a given axis. This expression can be shown in

$$q = cos\left(\frac{\alpha}{2}\right) + sin\left(\frac{\alpha}{2}\right) * v \tag{5}$$

The quaternion must have unit norm to correctly represent a rotation. The quaternion norm is given by

$$|q| = \sqrt{q_0^2 + q_1^2 + q_2^2 + q_3^2} \tag{6}$$

The angular rotation is subsequently converted from the quaternion to the Euler angle version using standard formulas. In this case, the *X Y Z* sequence of Euler angles was chosen. Based on this form, the roll, pitch, and yaw angles can be expressed as

$$\varphi = atan^2\left(2\left(q_2q_3 + q_0q_1\right), \left(q_0^2 - q_1^2 - q_2^2 - q_3^2\right)\right) \tag{7}$$

$$\theta = asin\left(\frac{2\left(q_0q_2 - q_1q_3\right)}{\left(q_0^2 + q_1^2 + q_2^2 + q_3^2\right)}\right) \tag{8}$$

$$\psi = atan^2\left(2\left(q_1q_2 + q_0q_3\right), \left(q_0^2 + q_1^2 - q_2^2 - q_3^2\right)\right) \tag{9}$$

The state equation in the time-continuous form can be expressed by

$$\dot{q}_n^b = \frac{1}{2}\Omega_{nb}^n q_n^b \tag{10}$$

where the quaternion q_n^b represents the rotation of the body frame, united to the IMU sensor, with respect to the inertial *n*-frame. Besides, the rotational matrix Ω_{nb}^n is derived from the quaternion's properties

$$\Omega_{nb}^n = \begin{bmatrix} 0 & -w_x & -w_y & -w_z \\ w_x & 0 & w_z & -w_y \\ w_y & -w_z & 0 & w_x \\ w_z & w_y & -w_x & 0 \end{bmatrix} \tag{11}$$

In the matrix (10), w_x, w_y, w_z are the angular velocities measured by the gyroscope sensor. The gyro data are used to determine the matrix deriving the evolution of the system from the previous state. Consequently, there is no explicit external input with the evolution law u_k. B_k [see (2)] and thus a time-varying $A_{\mathrm{TC}} = (1/2)\Omega_{nb}^n$ matrix was obtained. The time-continuous form can be written as in (11) by making explicit the derivative operation

$$\dot{q}_n^b = \lim_{T\to 0}\frac{q_n^b\left(t+T\right) - q_n^b\left(t\right)}{T} = A_{\mathrm{TC}}q_n^b\left(t\right) \tag{12}$$

For the digital Kalman Filter implementation, we need to convert Eq. (11) to a discrete-time one with using the time step *T* between each execution of the algorithm. As a result, we derive

$$q_n^b\left(t+T\right) = q_n^b\left(t\right) + A_{\mathrm{TC}}q_n^b\left(t\right)T = \left(I + A_{\mathrm{TC}}T\right)q_n^b\left(t\right) \tag{13}$$

A_k is the discrete-time matrix with the form shown in

$$A_k = \left(I + A_{\mathrm{TC}}T\right) = \left(I + \frac{1}{2}\Omega_{nb}^n T\right) \tag{14}$$

The quaternion norm is not preserved in the state equation. As the angle position can be correctly represented only with unit quaternions, a normalization unit was thus used to ensure data integrity.

As mentioned earlier, the angular position is updated using Eq. (2) with gyro data only. Therefore, we need to determine the correction equation of the Kalman Filter. Basically, there are two correction equations in our system, one for each stage: the first correction stage uses data from the accelerometers to correct the system state and the second correction stage uses data from the magnetic compass. Using the Kalman Filter theory, the correction equation can be calculated with the following

$$\widehat{x}_k = \widehat{x}_k^- + K_k\left(z_k - H\widehat{x}_k^-\right) \tag{15}$$

In Eq. (14), the residual is derived from the difference between the actual measurement z_k., which is the accelerometer or the magnetic compass data, and the expected measurement $H\widehat{x}_k^-$ that is calculated from (2). In order to calculate a posteriori estimation of the system state $\widehat{x}_k$, the residual must be weighted with the Kalman gain K_k.. In addition, we used an extended Kalman Filter and the nonlinear relationship $h\left(\widehat{x}_k^-\right)$ to calculate the estimated gravity or the magnetic field (Sabatini 2006; Roetenberg et al. 2007).

The Kalman gain$K_k$is calculated with involving many matrix operations. Consequently, we need to define a priori noise covariance P_k^- in the state estimation using a priori state equation. This can be expressed as

$$P_k^- = A_kP_{k-1}A_k^{\mathrm{T}} + Q_{k-1} \tag{16}$$

where the matrix P_{k-1} is a posteriori noise covariance matrix at the previous filter iteration [see (17)], while the matrix A_k is the system evolution that contains the gyro data. In our system, the process noise covariance matrix Q_{k-1} is directly depending on the noise of the gyro and other gyro error sources. Additionally, the Q_{k-1}value is related to the noise during the system evolution.

In the extended Kalman Filter, the Kalman gain is estimated with the following

$$K_k = P_k^- H_k^{\mathrm{T}} \left(H_k P_k^- H_k^{\mathrm{T}} + V_k R_k V_k^{\mathrm{T}} \right)^{-1} \tag{17}$$

whereH_k and V_k are the Jacobian matrices of the partial derivatives with respect to the noise of the nonlinear equations h_1 and h_2 [see (18) and (22)] and to the quaternion. These equations relate the quaternion to the estimated gravity and magnetic field. Moreover, an Extended Kalman Filter is used in these equations owing to the nonlinearity of these equations. In this system, the measurement noise covariance matrixR_k directly depends on the accelerometer and magnetic sensor noises, also other error sources that are considered as noise.

At the end, it is necessary to define a posteriori error covariance matrix P_k to be used in the subsequent filter iteration.

$$P_k = (I - K_k H_k) P_k^- \tag{18}$$

The first correction stage in our system uses accelerometer data to correct the system state. To calculate the expected gravity vector, it is necessary to calculate the estimated angular position and is subtracted from the value measured from the accelerometer, obtaining the so-called residual. The direction cosine matrix R_n^b in Eq. (19) is used to calculate the estimated gravity vector $\widehat{g}$ with the *g*–force acceleration $|g|$ constant.

$$h_1(q_k) = \widehat{g} = R_n^b \begin{bmatrix} 0 \\ 0 \\ |g| \end{bmatrix} = |g| \begin{bmatrix} 2q_1q_3 - 2q_0q_2 \\ 2q_0q_1 + 2q_2q_3 \\ q_0^2 - q_1^2 - q_2^2 + q_3^2 \end{bmatrix} \tag{19}$$

$$R_n^b = \begin{bmatrix} q_0^2 + q_1^2 - q_2^2 - q_3^2 & 2q_1q_2 + 2q_0q_3 & 2q_1q_3 - 2q_0q_2 \\ 2q_1q_2 - 2q_0q_3 & q_0^2 - q_1^2 + q_2^2 - q_3^2 & 2q_2q_3 + 2q_0q_1 \\ 2q_1q_3 + 2q_0q_2 & 2q_2q_3 - 2q_0q_1 & q_0^2 - q_1^2 - q_2^2 + q_3^2 \end{bmatrix} \tag{20}$$

Apart from measuring gravity, the accelerometer is also used to measure the external accelerations in a dynamic state. However, this tends to make the measured gravity suffers from significant errors. Thus, the residual must be weighted with theK_{k1}gain which is a coefficient calculated from the statistics of the noise covariance matrices of the system. The Jacobian matrix $H_{k1}$of the Kalman gain is calculated with:

$$H_{k1} = \frac{\partial h_{1[i]}}{\partial q_{|j|}} = \begin{bmatrix} -2q_2 & 2q_3 & -2q_0 & 2q_1 \\ 2q_1 & 2q_0 & 2q_3 & 2q_2 \\ 2q_0 & -2q_1 & -2q_2 & 2q_3 \end{bmatrix} \tag{21}$$

The current angular position is not affected by the accelerometer noise as well as the magnetic compass noise. Therefore, the Jacobian matrix V_k is an identity matrix. The roll and pitch angles can be easily corrected with the gravity vector measurement. To ensure the applicable corrections do not influence yaw estimation, the third vectorial part of the correction quaternion $q_{\epsilon 1}$ is set equal to zero.

$$q_{\epsilon 1} = q_{\epsilon 1,0} + q_{\epsilon 1,1} + q_{\epsilon 1,2} + 0 \cdot q_{\epsilon 1,3} \tag{22}$$

In the second stage of our method, we used the same algorithm but using different noise covariance matrices to calculate a second K_{k2} gain. The magnetic field, normalized to one, is considered directed along the *y*.–axis only, and the vertical component is neglected. It is owing to the Earth's magnetic field has a variable intensity from 0.25 to 0.65 G and the vertical component is geographically dependent. The magnetic field of the Kalman Filter is calculated with the following

$$h_2(q_k) = \widehat{m} = R_n^b \begin{bmatrix} 0 \\ 1 \\ 0 \end{bmatrix} = \begin{bmatrix} 2q_1q_2 + 2q_0q_3 \\ q_0^2 - q_1^2 - q_2^2 - q_3^2 \\ 2q_2q_3 - 2q_0q_1 \end{bmatrix} \tag{23}$$

The Jacobian matrix H_{k2} is calculated with the following

$$H_{k2} = \frac{\partial h_{2[i]}}{\partial q_{|j|}} = \begin{bmatrix} 2q_3 & 2q_2 & 2q_1 & 2q_0 \\ 2q_0 & -2q_1 & -2q_2 & -2q_3 \\ -2q_1 & -2q_0 & 2q_3 & 2q_2 \end{bmatrix} \tag{24}$$

In this case, only yaw angle is affected by magnetic anomalies while others are not. Therefore, the first two vectorial parts of the correction quaternion $q_{\epsilon 2}$ are set equal to zero.

$$q_{\epsilon 2} = q_{\epsilon 2,0} + 0 \cdot q_{\epsilon 2,1} + 0 \cdot q_{\epsilon 2,2} + q_{\epsilon 2,3} \tag{25}$$

4 Experimental results

This section outlines the simulation results of the system's performance using the Extended Kalman Filter (EKF) algorithm. The experiment was conducted to evaluate the system's performance while moving along a path mainly composed of straight lines that are 6 m in length. Moreover, the experiment used real data acquired by an Ambubot while navigating an indoor environment located on the fourth floor of National Taipei University Humanity building. The

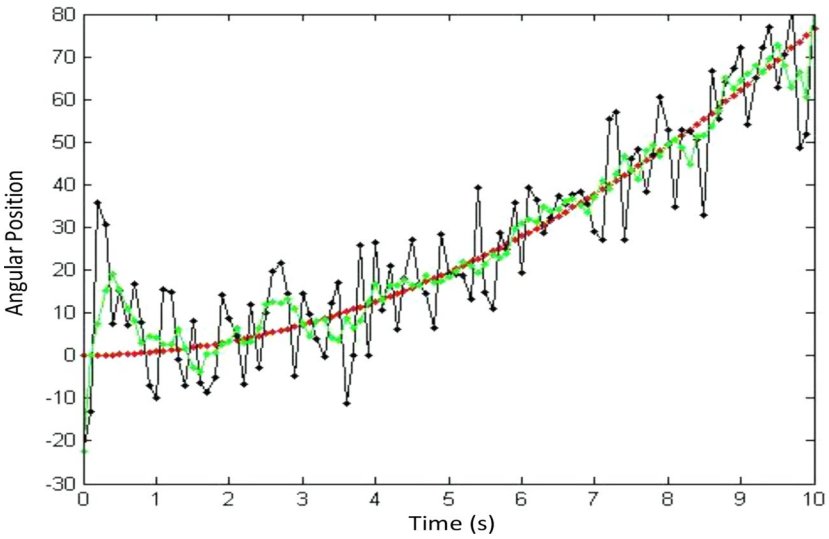

Fig. 13 The plot of measured angular position and estimated angular position using a moving average

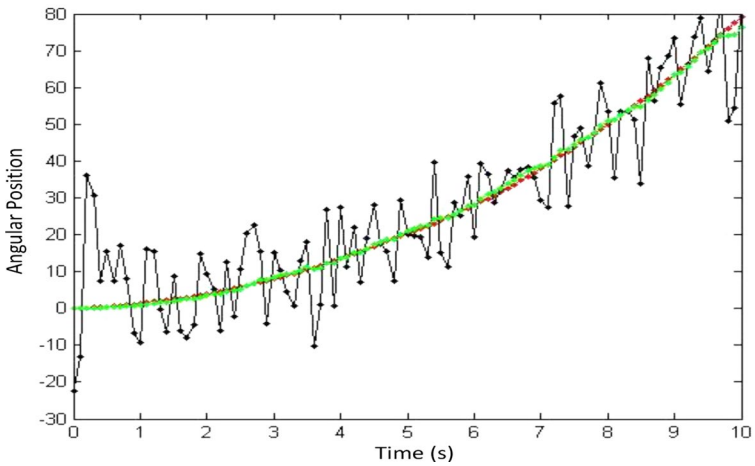

Fig. 14 The plot of measured angular position and estimated angular position using the EKF

system's performance was evaluated to confirm the accurate estimation of the initial position. The data collection was carried out using a laptop mounted on the Ambubot, which also sent commands to the robot.

The position of Ambubot is calculated using data collected by its IMU, which provides acceleration, gyroscope, and magnetic compass data. These data are gathered during Ambubot's navigation and are used as input to the simulation program. The angular displacement results obtained by applying the EKF to the IMU data are shown in Figs. 13 and 14. The true position of Ambubot is represented by a red line, the EKF estimate by a green line, and the noisy IMU measurements by the remaining curve. The IMU is highly sensitive to its surroundings. Therefore, to assess Ambubot's comparative performance, we ran the program in Matlab using two different methodologies: a moving average approach and the EKF. Table 1 displays the angular displacement between the measured and estimated positions obtained from each method.

Figure 13 illustrates the angular displacement of Ambubot obtained by applying the moving average methodology. It is noteworthy that the instantaneous errors between the measured and estimated positions are considerably large. Unlike the EKF, the moving average technique does not continuously update the angular position to produce a more accurate estimation, even though its overall performance is acceptable on average.

In Fig. 14, the angular estimation of Ambubot based on the EKF is presented. It can be observed that the errors derived from the EKF are smaller in comparison to those obtained from the moving average technique. This can be attributed to the two correction stages of the EKF utilized in our system. As a result, the EKF provides position estimates that are nearly identical to the measured data. Moreover, the application of the EKF technique enables the correction of angular position errors that arise from the IMU, leading to accurate localization of Ambubot.

Any bias present in the IMU sensor's output can have a direct impact on the accuracy of the Ambubot's position

Table 1 Comparison of the angular displacement errors in different approaches

Time/s	Angular Position (Radian)	Moving Average		EKF		EKF (Bias: 2.05)	
		Estimated	Error	Estimated	Error	Estimated	Error
1	1.8	4.8	3	1.78	0.02	1.8	0
2	4.3	4.3	0	4.28	0.02	4.35	0.05
3	8.6	8.6	0	8.65	0.05	10	1.4
4	12.7	17.4	4.7	12.7	0	12.71	0.01
5	20	19.5	0.5	20.18	0.18	20	0
6	28.8	30.9	2.1	28.8	0	27.9	0.9
7	39.4	38.2	1.2	39.46	0.06	39.5	0.1
8	50.2	50.2	0	50.3	0.1	51.1	0.9
9	62.1	63.9	1.8	62.1	0	62.4	0.3
10	77.5	77.8	0.3	76.8	0.7	76.5	1

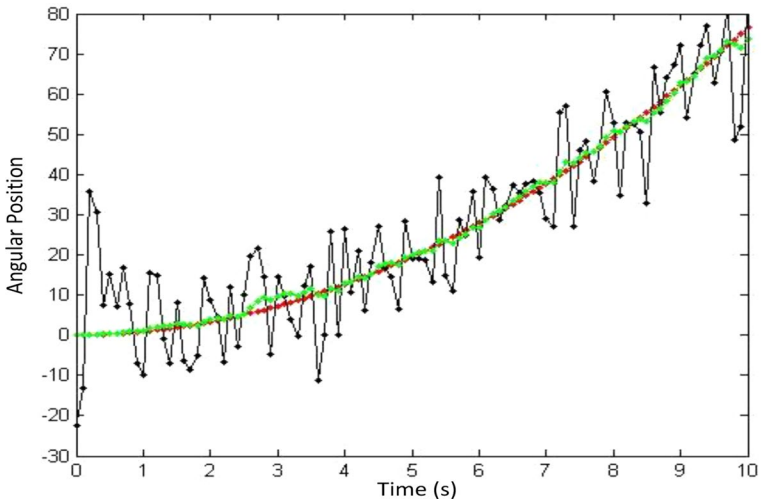

Fig. 15 The plot of measured angular position and estimated angular position using the EKF by adding the measurement bias of accelerometer 2.05

estimation. However, when a bias was introduced to the accelerometer, as shown in Fig. 15, the estimation position of Ambubot was not significantly affected, and the performance remained superior to that of the moving average technique. Overall, the EKF method performed satisfactorily in our system, even when a bias was present in the IMU sensor's output. Although the experiments were conducted in an offline manner, it was evident that the EKF method is highly effective and can be implemented in real-time scenarios.

5 Conclusion

The dispatch process of Ambubot to victim locations can be achieved through tele-control, partially autonomous, or fully autonomous methods. In tele-control, a remote operator uses a remote control device to steer Ambubot and monitors the live video stream from two surveillance cameras to locate and approach the victim. In contrast, Ambubot operates in autonomous navigation and obstacle avoidance mode in partially and fully autonomous methods. The primary difference between these two methods lies in the execution of AED. In fully autonomous mode, Ambubot carries out the AED on its own without any human intervention, while in partially autonomous mode, laypeople must apply the AED pads to the victim's bare chest.

During the system modeling and design, we developed an Extended Kalman Filter as a sensor fusion algorithm, and we used quaternions to represent angular position data. Quaternions offer more flexibility than Euler angles, as they can be easily linearized and converted to other rotation representation methods. To enhance flexibility and simplify our system, we utilized two correction stages of the EKF. The first correction stage uses accelerometer data to correct the system state, while the second correction stage employs magnetic compass data for angular position correction. Our simulation results show that the EKF performed well with Ambubot, with a smaller error effect on the angular position compared to the moving average technique.

Author contributions Conceptualization, C.Y.and C.L.; methodology, C.Y. and H.S.; validation, C.Y., H.S., Z.T; formal analysis, C.Y., H.S., Z.T; resources, C.Y. and C.L.; writing—original draft preparation, C.Y., H.S., Z.T; writing—review and editing, C.Y., H.S., Z.T; supervision, C.L.; project administration, C.L.; funding acquisition, C.L.

Data availability No datasets were generated or analysed during the current study.

Declarations

Competing interests The authors declare no competing interests.

References

Arif, M., Samani, H.A.M.B.U.B.O.T.: Ambulance robot automated external defibrillator robotic ambulance. *In Proc. 16th Int. Conf. Adv. Commun. Technol*. 58–66 (2014)

Arif, M., Samani, H., Yang, C.Y., et al.: Adaptation of mobile robots to intelligent vehicles. *IEEE*. 550–553, (2012)

Bai, Y.T., Yan, B., Zhou, C.G., et al.: State of art on state estimation: Kalman filter driven by machine learning. Annu. Rev. Control. **56**, 100909 (2023)

Bird, J., Arden, D.: Indoor navigation with foot-mounted strapdown inertial navigation and magnetic sensors. IEEE Wirel. Commun. **18**(2), 28–35 (2011)

Chang, H.L., Shen, Q., Zhou, Z.G., et al.: Design, fabrication, and testing of a bulk Micromachined Inertial Measurement Unit. Sens. **10**(4), 3835–3856 (2010)

Cheng, Y., Zhang, S.K., Wang, X.Y., et al.: Kalman Filter with Adaptive Covariance Estimation for Carrier tracking under weak signals and dynamic conditions. Electron. **13**(7), 1288 (2024)

Hu, L.L., Bao, Y., Sun, Z., et al.: Outlier detection based on Nelder-Mead Simplex Robust Kalman Filtering for Trustworthy Bridge Structural Health Monitoring. Remote Sens. **15**(9), 2385 (2023)

Karlsson, L., Hansen, C.M., Vourakis, C., et al.: Improving bystander defibrillation in out-of-hospital cardiac arrests at home. Eur. Heart J. Acute Cardiovasc. Care. **9**, S74–S81 (2020)

Kim, A., Golnaraghi, M.F.: A quaternion-based orientation estimation algorithm using an inertial measurement unit. *Position Location and Navigation Symposium*, *2004. PLANS 2004. IEEE*. 268–272. (2004)

Liu, Y.H., Fan, X.Q., Lv, C., et al.: An innovative information fusion method with adaptive Kalman filter for integrated INS/GPS navigation of autonomous vehicles. Mech. Syst. Signal. Process. **100**, 605–616 (2018)

Liu, R., Liu, W.L., Liu, Y.X., et al.: Modeling and Optimization for Emergency Medical Services Network. IEEE Trans. Autom. Sci. Eng. **19**(4), 3520–3535 (2022)

Lyu, X.X., Duan, P.H., Duan, Z.S., et al.: Stability Analysis of Constrained Distributed Nonlinear and Linear Kalman Filters for Dynamical Systems with State constraints. IEEE Trans. Aerosp. Electron. Syst. **60**(1), 632–643 (2024)

Moraes, D., Luiz, O.: Some evidence on the reduction of the disasters impact due to natural hazards in the Americas and the Caribbean after the 1990s. Int. J. Disaster Risk Reduct. **75**, 102984 (2022)

Roetenberg, D., Slycke, P.J., Veltink, P.H.: Ambulatory position and orientation tracking fusing magnetic and inertial sensing. IEEE Trans. Biomed. Eng. **54**(5), 883–890 (2007)

Rothmier, J.D., Drezner, J.A.: The role of automated external defibrillators in athletics. Sports Health. **1**(1), 16–20 (2009)

Sabatini, A.M.: Quaternion-based extended Kalman filter for determining orientation by inertial and magnetic sensing. IEEE Trans. Biomed. Eng. **53**(7), 1346–1356 (2006)

Samani, H., Zhu, R.B.: Robotic automated external defibrillator ambulance for emergency medical service in smart cities. IEEE Access. **4**, 268–283 (2016)

Tan, C.W., Park, S.: Design of accelerometer-based inertial navigation systems. IEEE Trans. Instrum. Meas. **54**(6), 2520–2530 (2005)

Von der Hardt, H.J., Arnould, P., Wolf, D., et al.: A method of mobile robot localisation by fusion of odometric and magnetometric data. INT. J. ADV. MANUF. TECH. **9**(1), 65–69 (1994)

Xiao, Y., Jiang, T., Fan, G.W., et al.: A meticulous covariance adaptive Kalman filter for satellite attitude estimation. Meas. Sci. Technol. **35**(4), 045104 (2024)

Xu, X.L., Sun, Y.J., Tian, X.C., et al.: A novel orientation determination Approach of Mobile Robot using Inertial and magnetic sensors. IEEE Trans. Ind. Electron. **70**(4), 4267–4277 (2023)

Yuri, X.P., Bachmann, E.R., McGhee, R.B.: A simplified quaternion-based algorithm for orientation estimation from earth gravity and magnetic field measurements. IEEE Trans. Instrum. Meas. **57**(3), 638–650 (2008)

Zanetti, R., Majji, M., Bishop, R.H., et al.: Norm-Constrained Kalman Filtering. J. Guidance Control Dyn. **32**(5), 1458–1465 (2009)

Zhang, Y., Xue, W.C., Sun, L., et al.: Extended state Kalman filter-based path following control of underactuated autonomous vessels. Trans. Inst. Meas. Control. **43**(15), 3311–3321 (2021)

Dr. Chan-Yun Yang is the Director of the Intelligent Modeling and Control Lab and Professor with the Department of Electrical Engineering, College of Electrical Engineering and Computer Science, National Taipei University, Taiwan. His career in robotics and artifcial intelligence research has spanned many countries. He was awarded a Ph.D. degree from the Department of Bio-Industrial Mechatronics Engineering, National Taiwan University. After obtaining his Ph.D. degree he became a Research Fellow at the Keio-NUS CUTE Centre, which is a collaborative research center with locations in both the National University of Singapore (NUS) and Keio University in Japan. He is also actively serving several robotics and AI related journals and conferences as Editorial Board member, Organizing.

Hooman Samani is Lecturer in machine learning, Al for robotics at the School of Engineering, Computing and Mathematics, University of Plymouth, UK. He has worked as Associate Professor and Founder and Director of the AIART Lab at the National Taipei University of Taiwan. He holds a Ph.D. degree in robotics from the National University of Singapore (NUS) and has worked as Research Fellow at the Keio-NUS CUTE Centre, a joint research centre between NUS and Keio University of Japan. He is actively serving in several robotics and Al related journals and conferences as editorial board member, organizing committee member, workshop organizer and reviewer.

Zirong Tang received his master's degree from the School of Mechanical and Electrical Engineering at Hohai University in 2024. His research interests include machine learning, numerical simulation, and surface enhancement. He is proficient in Python, Matlab, and Abaqus software.

Dr Chunxu Li is a senior lecturer at the School of Aerospace, Civil, Electrical, General Engineering and Mechanical Engineering, Swansea University. He was appointed as a lecturer at the School of Engineering, Computing and Mathematics, University of Plymouth from 2020 - 2023. He has published over 40 academic papers, and won the Best Student Paper Award and was shortlisted for the Best Paper Award in IEEE international conferences. He has expertise in ROS, JAVA, C++, Python and MATLAB with over 8 years working experience on multiple robot platforms, e.g., KUKA iiwa, Baxter, NAO, Universal, etc. Dr Li is an Associate Fellow of the Higher Education Academy and a member of IEEE (Institute of Electrical and Electronics Engineers). As the PI and the main co-I, he successfully granted a number of projects and fundings.